PCCP

Energetics of CO_2 and H_2O adsorption on alkaline earth metal doped TiO_2

Journal:	*Physical Chemistry Chemical Physics*
Manuscript ID	CP-ART-04-2020-001787.R2
Article Type:	Paper
Date Submitted by the Author:	17-Jun-2020

Complete List of Authors:	da Silva, Andre Luiz; Universidade de São Paulo, Department of Metallurgical and Materials Engineering Wu, Lili; University of California at Davis, NEAT ORU and Thermochemistry Facility Caliman, Lorena Batista; Universidade de São Paulo, Department of Metallurgical and Materials Engineering Castro, Ricardo; University of California at Davis, Chemical Engineering and Materials Science Navrotsky, Alexandra; Arizona State University, School of Molecular Sciences and Center for Materials of the Universe Gouvea, Douglas; University of Sao Paulo, Metallurgical and Materials Engineering

SCHOLARONE™
Manuscripts

ARTICLE

Energetics of CO_2 and H_2O adsorption on alkaline earth metal doped TiO_2

Received 00th January 20xx,
Accepted 00th January 20xx

DOI: 10.1039/x0xx00000x

Andre Luiz da Silva,*[a] Lili Wu, [b] Lorena Batista Caliman, [a] Ricardo H.R. Castro, [c] Alexandra Navrotsky [d] and Douglas Gouvêa [a]

The process of CO_2 and H_2O adsorption on the surface of nano-oxide semiconductors is important in the overall performance of artificial photosynthesis and other applications. In this study, we explored the thermodynamics of CO_2 and H_2O adsorption on TiO_2 as a function of surface chemistry. We applied gas adsorption calorimetry to investigate the energetics of adsorption of those molecules on the surface of anatase nanoparticles. In an attempt to increase TiO_2 surface affinity to CO_2 and H_2O, TiO_2 was doped with alkaline earth metals (MgO, CaO, SrO, and BaO) by manipulating the chemical synthesis. Adsorption studies using diffuse reflectance infrared spectroscopy at different temperatures indicate that due to the segregation of alkaline earth metals on the surface of TiO_2 nanoparticles, both CO_2 and subsequent H_2O adsorption amounts could be increased. CO_2 adsorbs in two different manners, forming carbonates which can be removed at temperatures lower than 700 °C, and a more stable linear adsorption that remains even at 700 °C. Additionally to the surface energetic effects, doping also increased specific surface area, resulting in further improve in net gas adsorption.

Introduction

CO_2 conversion to marketable organic molecules via photocatalytic processes (artificial photosynthesis – AP) is one of the most attractive strategies for CO_2 capture while serving as an effective way to exploit solar power.[1,2] However, due to the energetically unfavorable nature of photoreduction processes and the thermodynamically stable nature of the CO_2 molecule, advanced photocatalysts are necessary to facilitate the CO_2 photoreduction and increase the solar energy conversion efficiency.[3] The CO_2 molecule is stable and chemically inert due to its electronic and geometric properties.[4] The dissociation energy of C=O is 750 kJ/mol, while C-H and C-C bonds are 430 and ~336 kJ/mol, respectively.

Catalytically assisted AP is a process that involves the CO_2 photoreduction and the oxidation of H_2O molecules occurring in two steps: firstly, CO_2 and H_2O are adsorbed onto the catalyst surface, a process that benefits from high surface area materials and low physical and chemical energy barriers for adsorption. Secondly, the photocatalytic process is induced with excitons from photons which initiate the photoreduction process.[3] The productivity of this process is directly influenced by (1) the adsorption of the gas molecules, (2) light absorption, and (3) charge separation.[3] In the present study, we focus our attention on improving the adsorption of gas molecules, such as CO_2 and H_2O.

TiO_2 is one of the most interesting materials used for this purpose due to its abundance, chemical stability, and appropriate electronic absorption spectrum.[1,5,6] The most reported products of CO_2 photoreduction with water on TiO_2 are CH_4, CO, H_2, and CH_3OH. This selectivity is related to the band position relative to the redox potentials.[6] However, to properly use the solar energy on CO_2 photoreduction, some limitations of the TiO_2 nanoparticles have to be overcome, such as their large bandgap, which leads to low solar energy usage, fast charge recombination rates that decrease the photocatalytic performance, and the relatively insufficient CO_2 adsorption capability.[7]

CO_2 adsorption on TiO_2 surfaces has been reported to take place in the physisorbed (without chemical dissociation) and chemisorbed (with dissociation and reaction taking place) modes. The former is usually observed on pristine TiO_2 surfaces,[8] while the second is more common on reduced or oxidized TiO_2 surfaces.[9–10] It is difficult for CO_2 to bind in chemisorption mode to a pristine TiO_2 surface without the existence of hydroxyl groups or defects. This is because CO_2 is a fairly inert molecule with the reduction potential of CO_2/CO_2^- of about -1.9 eV, which is much higher than that of the TiO_2

[a] Department of Metallurgical and Materials Engineering, Polytechnic School - University of São Paulo, São Paulo 05508-030, Brazil.
E-mail: andresilva.urussanga@gmail.com, andresilva.urussanga@usp.br;
Tel: +55 11 30916087
[b] Department of Chemistry and NEAT ORU, University of California, Davis, One Shields Avenue, Davis, CA 95616, United States.
[c] Department of Materials Science and Engineering, University of California, Davis, One Shields Avenue, Davis, CA 95616, United States.
[d] School of Molecular Sciences and Center for Materials of the Universe, Arizona State University, Tempe AZ 85287 United States.

† Footnotes relating to the title and/or authors should appear here.
Electronic Supplementary Information (ESI) available: [details of any supplementary information available should be included here]. See DOI: 10.1039/x0xx00000x

conduction band, preventing electron transfer from TiO_2 to CO_2.[11]

One of the attempts to overcome the somewhat insufficient CO_2 adsorption capability on TiO_2 is the use of a foreign element that tends to increase the CO_2 adsorption. Liu et al.[12] studied the CO_2 photoreduction with H_2O vapor by porous MgO-TiO_2 microspheres. The MgO-TiO_2 presented a higher production rate of CO comparing to pristine TiO_2. In situ DRIFTS analysis on CO_2 adsorption and photo-reduction showed the formation of more active bicarbonate species but less poisoning carbonate species on the Mg/Ti surface. The process was also benefited by the easier and faster desorption/conversion of the reaction intermediate.[12] Wang et al.[13] also showed an increment in the photocatalytic reduction of CO_2 with H_2O vapor into hydrocarbon fuel using MgO-TiO_2 nanostructures as photocatalysts. The increment on CH_4 production was mainly attributed to the improved CO_2 adsorption and activation through incorporated MgO.

Even though those studies have shown that MgO has improved the CO_2 adsorption on TiO_2 nanoparticles, there is still a limited understanding of the thermodynamics of the competitive CO_2 and H_2O adsorption processes. In the context of AP, it is necessary to assure a balanced affinity of TiO_2 to both CO_2 and H_2O. Thus, to better understand the dependencies of adsorption, here we present a detailed study on CO_2 and H_2O adsorption on undoped and alkaline earth metals doped TiO_2 nanoparticles. Based on previous studies,[14,12,13] we expect that those oxides (MgO, CaO, SrO, and BaO) increase the CO_2 adsorption on TiO_2 nanoparticles. The previously validated selective lixiviation method [15,16] was used to demonstrate and quantify segregation of alkalines to the surface of the TiO_2 nanoparticles, which was associated with a surface chemistry change, reduction in crystallite sizes, and increase the specific surface area. The detailed gas adsorption studies were performed on a Micromeritics ASAP 2020 instrument coupled with a Calvet-type microcalorimeter. Diffuse reflectance infrared Fourier transform (DRIFT) spectroscopy at different temperatures was used to detect the species adsorbed on the surface of TiO_2. Moreover, the nanopowders were characterized by XRD, density, SSA, and chemical composition.

Experimental

Synthesis of undoped and doped TiO_2 nanoparticles.

TiO_2-based powders containing MgO, CaO, SrO, or BaO were synthesized by the polymeric precursor method. The titanium-oxide polymeric precursor was prepared by mixing titanium isopropoxide (19.4 wt %) with ethylene glycol (45.4 wt %) at 40 °C, followed by heating to 70 °C and addition of citric acid (35.2 wt %). Then, the solution was heated to 120 °C for polyesterification. The addition of MgO, CaO, SrO, or BaO was made using acid solutions (0.2 mol/L) of each dopant. These solutions were obtained by solubilizing the appropriate amount of $Mg(NO_3)_2$, $Ca(NO_3)_2$, $Sr(NO_3)_2$, or $Ba(NO_3)_2$ in an aqueous nitric acid solution (0.1 M), followed by chemical analysis.

The samples were prepared by mixing calculated amounts of the solutions and the precursor, with the target molar concentration of 5.0 %. The doped samples were labeled as Ti050Mg, Ti050Ca, Ti050Sr, and Ti050Ba, which stands for TiO_2 doped with MgO, CaO, SrO, and BaO, respectively. The calcination was performed in two steps, the first one to decompose the organic trace, each sample was held at 350 °C for 4 h. Then, the powders were manually ground with a mortar and pestle and treated in the air at 350 °C for 15 h to complete the oxidation and particle size stabilization.

Sample characterization.

The powder X-ray diffraction patterns were obtained using a Philips X´Pert PRO PW 3040/00 diffractometer with Cu Kα radiation at 0.02° steps per second over the 2θ range of 5-90 °. The lattice parameters were calculated using X´Pert Highscore software and the crystallite sizes were calculated using whole profile fitting using Materials Studio 6.0 software with CaF_2 and anatase structures as standards. The chemical compositions were analyzed by inductively coupled plasma atomic emission optical spectroscopy (ICP OES) using a Spectro Across spectrometer. The samples were prepared by melting the powders with sodium borate, followed by acid digestion. The powder density was obtained using a Micrometrics AccuPyc II 1340 gas pycnometer after 200 purges for degassing. Specific surface area measurements were carried out using the Brunauer, Emmett, and Teller (BET) method with nitrogen gas adsorption (77 K) (Micromeritics Gemini VII). The samples were degassed at 300 °C for ~16 h using a Micromeritics VacPrep 061 before the experiment.

Selective lixiviation and retreatment.

The surface excess of the dopants on TiO_2 nanoparticles was directly determined by superficial lixiviation performed by ultrasonicating ~100 mg of powder with 2 g of 0.1 M HNO_3 solution (pH = 1) for 1 h. Then, the samples were centrifuged at 13,000 rpm (~10,390g) for 20 min. Approximately 1 g of the supernatant solution was collected, diluted in ~10 g of H_2O, and analyzed by inductively coupled plasma atomic emission optical spectroscopy (ICP OES) using a Spectro Across spectrometer. In our previous study,[14] we have shown that the dopant has an equilibrium distribution between the surface and GB interfaces governed by a parameter similar to a chemical equilibrium constant. That is, if the additive is removed from the surface of the nanoparticles and then retreated (thermal activation), atoms located at the grain boundaries that could not be washed off will redistribute to find a new equilibrium. A portion of the dopants that are segregated in the GB will diffuse to the surface to minimize the total energy of the system. Thus, in the present study, we have retreated the lixiviated powders inside the ASAP 2020 before the CO_2 adsorption procedure. This procedure was performed to have a pristine surface of the nanopowders. The retreatment procedure was carried out at 250 °C for 4 h under vacuum, and at 350 °C for 15 h under oxygen to allow the

This journal is © The Royal Society of Chemistry 20xx

Please do not adjust margins

surface to be rebuilt without potential contaminations like carbonates that would overestimate the enthalpy of CO_2 adsorption. The same batches of lixiviated powders were also treated in a similar degassing system at the same conditions and characterized by X-ray diffraction, BET surface area, DRIFT absorption, and a new lixiviation procedure. The degassing condition was established by using thermogravimetry.

Diffuse reflectance infrared Fourier transform (DRIFT) spectroscopy was performed using a Thermo-Nicolet Magna 560 system with a scanning capacity from 500 to 5000 cm^{-1} and 4 cm^{-1} resolution. The analyses were carried out at room temperature, 350 °C, and 700 °C.

CO_2 and H_2O adsorption.

Gas adsorption isotherms and heats of adsorption were carried out simultaneously at 25 °C using a Micromeritics ASAP 2020 coupled with a Calvet-type microcalorimeter (Sensys Evo, Setaram). The instrument and methodology are described in detail elsewhere.[17] It was used about 35–80 mg of powder depending on the specific surface area of the sample, which provided a total surface area of ~3.5 m^2. The samples were placed in the chamber and degassed at 250 °C for 4 h under vacuum, and at 350 °C for 15 h under oxygen. The chamber was kept at 25 °C, and the dosing routine was programmed to be ~20 µmol CO_2 per dose. The instruments measure the enthalpy of CO_2 adsorption of the sample and the CO_2 coverage simultaneously. After the CO_2 adsorption procedure had finished, the chamber was evacuated for 6 h at 25 °C and H_2O adsorption took place. The H_2O dosing routine was programmed to be ~2 µmol H_2O per dose and equilibration time ~1.75 h for the first four doses, ~1 h for the fifth dose, ~0.75 h for sixth and seventh, and ~0.5 h from the eighth dose on. The equilibrium time was designed to be enough for the measured heat signal in the calorimeter to return to the baseline.

Results and discussion

Characterization of the nanoparticles.

The X-ray diffraction (XRD) patterns of samples subjected to the adsorption study are shown in Fig. 1. Anatase (JCPDS card no. 71-1167) was the predominant phase for all compositions. The observed broad peaks indicate nanosized crystallites. The broadening was higher on doped samples, which suggests smaller crystallite sizes. The broadening of doped samples increased as the ionic radius of the dopant increased.

The crystallite sizes, lattice parameters, density, and specific surface area (SSA) are shown in Table 1. The crystallite sizes (a = b, and c) decreased drastically for doped samples comparing to undoped one. This can be attributed to the effect of dopants on reducing the interfacial energies, consistently with the literature.[18,16,24–19] General coarsening models,[20] state that the particle size is directly proportional to interface energy (Eq. 1):

$$d_t^n - d_0^n = kD\sigma_i(t - t_0) \quad (1)$$

Here, the average particle size d_t is modified with time, t, d_0 is the average particle size at t_0, D is the diffusion coefficient, σ_i is the interface energy, k is a constant that depends on the approach to develop the kinetic equation, n is equal to 2, 3, or more and generally represents the mechanism of growth. The interface energy represents either the grain boundary or the surface of the material, and has been reported to be affected by interface segregation following Eq. 2:

$$\sigma_i = \sigma_0 + \Gamma_i \Delta H_{seg} \quad (2)$$

Here, σ_0 is the interface energy of the undoped nanopowders, ΔH_{seg} is the enthalpy of segregation, and Γ_i is the solute excess at the interface. This equation has only been proven reliable for systems with a single phase and low concentration of dopant.[14,21]

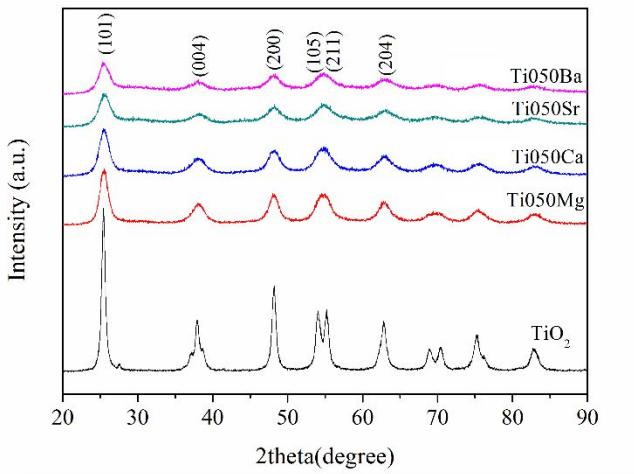

Fig. 1. X-ray diffraction patterns of samples after the lixiviation and retreatment procedure, undoped TiO_2 and doped with 5 mol% MgO, CaO, SrO, and BaO.

Table 1. Crystallite sizes, lattice parameters, density, and specific surface area (SSA).

Sample	Crystallite sizes a=b (nm)	Crystallite sizes c (nm)	Lattice parameters a=b (Å)	Lattice parameters c (Å)	Density (g/cm³)	SSA (m^2/g)
TiO_2	20.5±1.4	24.0±4.2	3.7773±0.0001	9.4818±0.0014	3.62±0.01	42.3±0.2
Ti050Mg	6.1±0.1	6.2±0.2	3.7621±0.0036	9.4109±0.0095	3.33±0.01	80.7±0.4
Ti050Ca	5.2±0.1	5.0±0.2	3.7516±0.0012	9.3770±0.0006	3.22±0.01	105.5±0.5

Ti050Sr	4.6±0.1	4.4±0.2	3.7604±0.0018	9.3889±0.0034	3.04±0.01	89.4±0.4
Ti050Ba	5.0±0.2	4.8±0.4	3.7622±0.0016	9.3873±0.0008	3.25±0.01	78.2±0.4

However, the kinetic parameters can be influenced by the dopants as well. If dopants are segregated to the interfaces, the mass movement towards, from, and across the interfaces is slowed down due to steric effects. Charge compensation defects (2+ replacing 4+ leading to oxygen vacancies) is another possible influencer of the kinetic parameters as it enhances oxygen total mobility, but this effect is considered limited in this system considering the cations and not oxygen, are the rate-limiting species.

The lattice parameters were reduced for all doped samples. The internal structure of small nanoparticles experiences high pressure due to surface stress, which can introduce lattice contraction or expansion. The surface stress is affected by the crystal structure, particle morphology and size, and nanoparticle surface state and surface environment (e.g. surface coating by organic molecules, or solutions with different compositions).[22] Lattice contraction on undoped TiO_2 has been observed as a function of particle size decrease for different synthesis methods, such as sol-gel using Ti ethoxide,[23,24] sol-gel using $TiCl_4$,[25,26] sol-gel using isopropoxide,[24] hydrolysis of Ti isopropoxide in supercritical fluid with HCl,[27] hydrolysis of Ti isopropoxide in supercritical water fluid,[28] and hydrolysis of titanium butoxide.[29] Doped TiO_2 nanoparticles have also experienced lattice contraction as a function of particle size decrease, e.g., ZnO-doped TiO_2,[22] and BaO-doped TiO_2.[14] Considering that all samples in the present study were synthesized using the same method, the lattice contraction can be related to the reduction in crystallite size, and with a change in the particle surface environments due to the surface segregation of the alkaline earth metals.

The densities of the powders measured by gas pycnometry are also shown in Table 1. Pure TiO_2 presented 3.62 g/cm³ density, which is slightly lower than the theoretical value of TiO_2 anatase (3.79 g/cm³). Doped samples showed a lower density comparing

with pristine TiO_2. This behavior has been attributed to a superficial structure disorder and gas adsorption, such as CO_2 and H_2O, which forms a superficial layer with lower density, decreasing the overall density of the system.[14]

The specific surface area (SSA) of pristine TiO_2 was 42.3 m²/g, while doped samples showed much higher values. This increment is a consequence of the interface segregation of the additives and it has the opposite trend than the crystallite sizes. CaO-doped TiO_2 showed the higher value, reaching 105.5 m²/g. The powders doped with MgO, SrO, and BaO, presented SSA of 80.7, 89.4, and 78.2 m²/g, respectively.

Chemical composition and surface excess of doped TiO_2 samples are shown in Table 2. The amount of dopant on the as-prepared nanopowders was close to target compositions. After the first lixiviation process, ~30 % of the dopants were removed from the samples. The samples with the remained dopants were used to perform the gas adsorption.

The excess of dopants on the surface was measured using the lixiviation method described in the experimental section and varied from 0.87 to 1.00 µmol/m². These are important data that explain the reduction in the crystallite sizes and the increment in the SSA shown in Table 1. They also show that the surface of TiO_2 is modified with the alkaline earth metals as we have predicted.

Table 2. Chemical composition before and after first lixiviation, and surface excess after lixiviation and retreatment.

Sample	Chemical composition before first lixiviation (mol % of dopant)	Chemical composition after first lixiviation (mol % of dopant)	Surface excess after lixiviation and retreatment (µmol/m²)
Ti050Mg	5.23	3.72	0.91±0.01
Ti050Ca	5.30	3.82	0.87±0.01
Ti050Sr	6.46	4.92	0.96±0.01
Ti050Ba	5.11	3.51	1.00±0.01

CO_2 and H_2O adsorption.

The first experiment performed to observe CO_2 and H_2O adsorption on the surface of undoped and doped TiO_2 was DRIFT absorbance (Fig. 2). The tests were performed at room temperature, 350 °C, and 700 °C. Peaks at ~940 cm^{-1} are commonly assigned to oxygen-metal bonding. The broad band from ~2500 to ~3700 cm^{-1} observed in all compositions at room temperature is assigned to stretching and bending modes of adsorbed water, which is typical in oxide nanoparticles and is associated with the capacity to adsorb H_2O and to the high SSA of the nanoparticles. At 350 °C and

This journal is © The Royal Society of Chemistry 20xx

Please do not adjust margins

700 °C, these H_2O bands disappeared due to the H_2O evaporation. The bands at ~1630 cm^{-1} can be either associated with H_2O or CO_2. At room temperature, the peaks are well defined for all compositions. However, it decreased at 350 °C and completely disappeared at 700 °C. The peak at 3690 cm^{-1} is associated with hydroxyl groups, which is common on TiO_2 nanoparticles.[21] At 350 °C, as the water evaporated, these peaks became more clearly visualized, with little difference among the samples. However, at 700 °C, the peaks disappeared for pure TiO_2 and MgO-doped TiO_2, and were seen with much smaller intensity for CaO, SrO, and BaO doped TiO_2. The modification of the TiO_2 with those elements may have created a stronger –OH adsorption site, which needs higher temperature to be released. The CO_2 adsorption bands observed in the present study are linear CO_2 adsorption which has a vibration at ~2330 cm^{-1}, and CO_2 associated with the carbonates, which are assigned at ~1570 cm^{-1} and ~1380 cm^{-1}. Both CO_2 adsorption species increased for doped samples. This is an effect of the TiO_2 surface modification with alkaline earth metals, which could have created adsorption sites that favor CO_2 adsorption. The linear CO_2 is seen even at 700 °C. It seems that a higher temperature would be needed to remove it from the TiO_2 surface, which due to the limitation of our apparatus, was not possible to perform. On the other hand, the CO_2 associated with the carbonates was still present at 350 °C, but it was gone at 700 °C. This indicates that these CO_2 species need less thermal energy to be released from the TiO_2 surface.

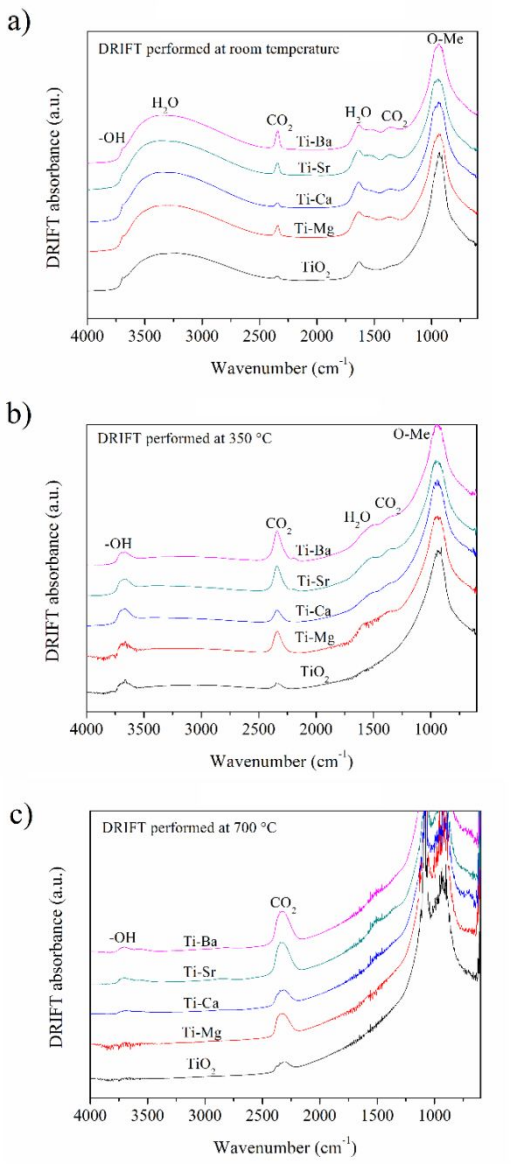

Fig. 2. DRIFT absorbance of the samples after the lixiviation and retreatment procedure for undoped TiO_2 and TiO_2 doped with 5 mol% MgO, CaO, SrO, and BaO. a) DRIFT performed at room temperature. b) DRIFT performed at 350 °C. c) DRIFT performed at 700 °C.

The CO_2 adsorption isotherms and differential heat of adsorption are shown in Fig. 3. Fig. 3a,b shows that pure TiO_2 has a behavior similar to the isotherm presented by Wu, et al.[30] for TiO_2 anatase. The lack of a clear inflection point, which is attributed to intermediate characteristics of type II and type III isotherms, suggests that a second adsorption layer might form before the completion of monolayer adsorption.[30] On the other hand, doped-TiO_2 samples presented a type III isotherm. When the adsorption was normalized by surface area, the difference between pure TiO_2 and doped samples was low. MgO, CaO, and BaO doped TiO_2 showed higher adsorption than TiO_2 above ~0.009 relative pressure, while SrO doped TiO_2 had smaller adsorption. Looking at the quantity adsorbed normalized by weight (Fig. 3b), it is observed that doped samples presented higher adsorption than pristine TiO_2. It

Please do not adjust margins

seems that the chemical modification of the TiO_2 surface partially covered with alkaline earth metals had a small contribution to the total CO_2 quantity adsorbed, while the increased SSA of doped samples played an important role by increasing the quantity adsorbed by ~2-3 times per gram of material, compared to pure TiO_2. The differential heat of adsorption did not show any significant difference among doped and undoped TiO_2 (Table 3). The differential enthalpies of the first dose were -50.4, -51.3, -50.33, and -49.9 kJ/mol for pure TiO_2, MgO, SrO, and BaO-doped TiO_2, respectively. The values were lower than those presented by Wu, et al.,[30] which was -59.4 kJ/mol for TiO_2 anatase. The integral enthalpies, which represent the overall heat effect caused by surface interactions were -36.4, -35.5, -35.4, and -34.7 kJ/mol for pure TiO_2, MgO, SrO, and BaO-doped TiO_2, respectively. These values are also lower than those presented by Wu, et al.,[30] which was -41.6 kJ/mol. An unexpected behavior on CaO-doped TiO_2 was observed. The enthalpy of adsorption on the first dose was -62 kJ/mol, while the integral enthalpy was -41.3 kJ/mol, which was more exothermic than other values found in this study.

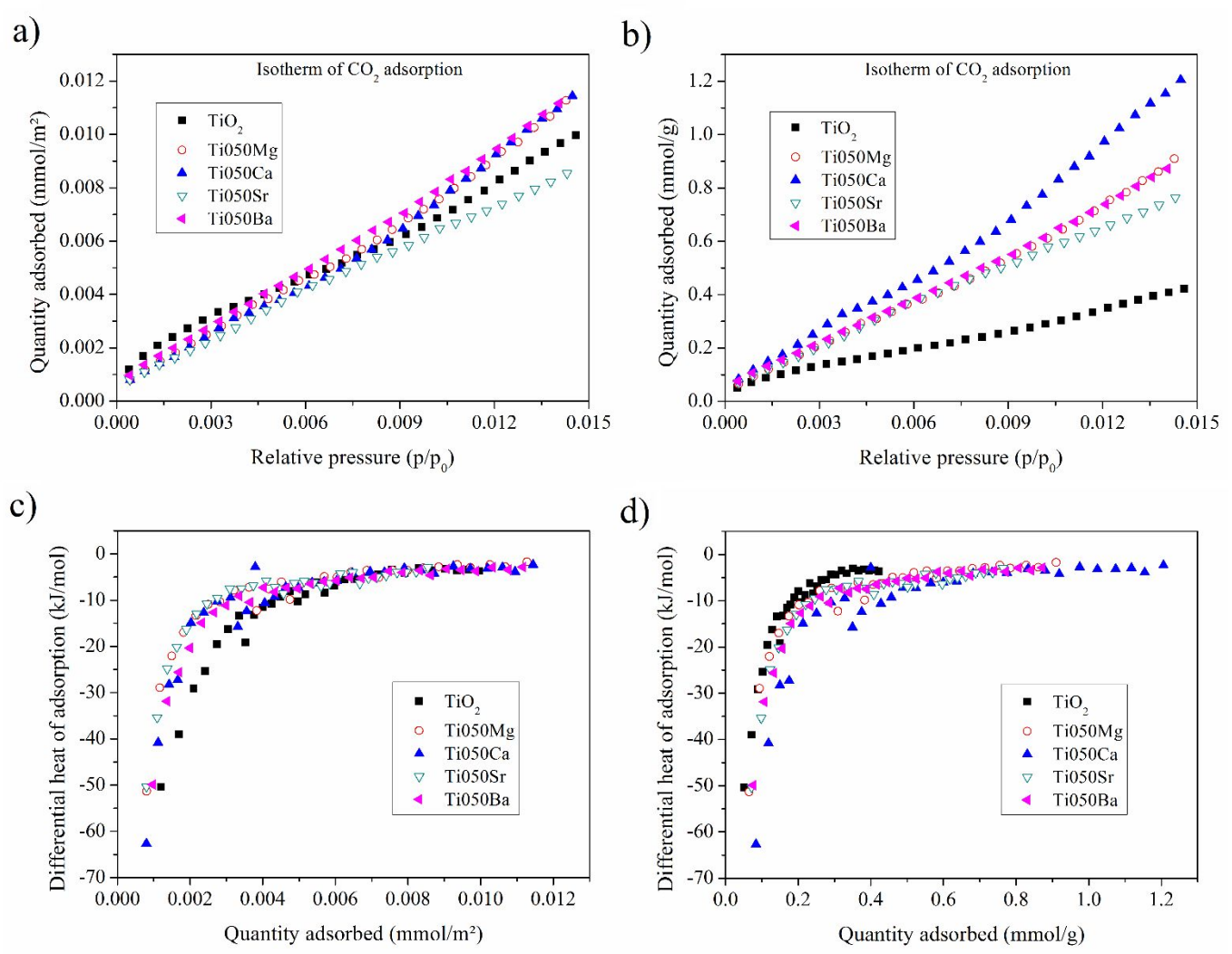

This journal is © The Royal Society of Chemistry 20xx

Please do not adjust margins

ARTICLE

Fig. 3. Isotherm of CO_2 adsorption normalized by surface area (a) and by weight (b). Differential heat of adsorption normalized by surface area (c) and by weight (d) for undoped TiO_2 and doped with 5 mol% MgO, CaO, SrO, and BaO.

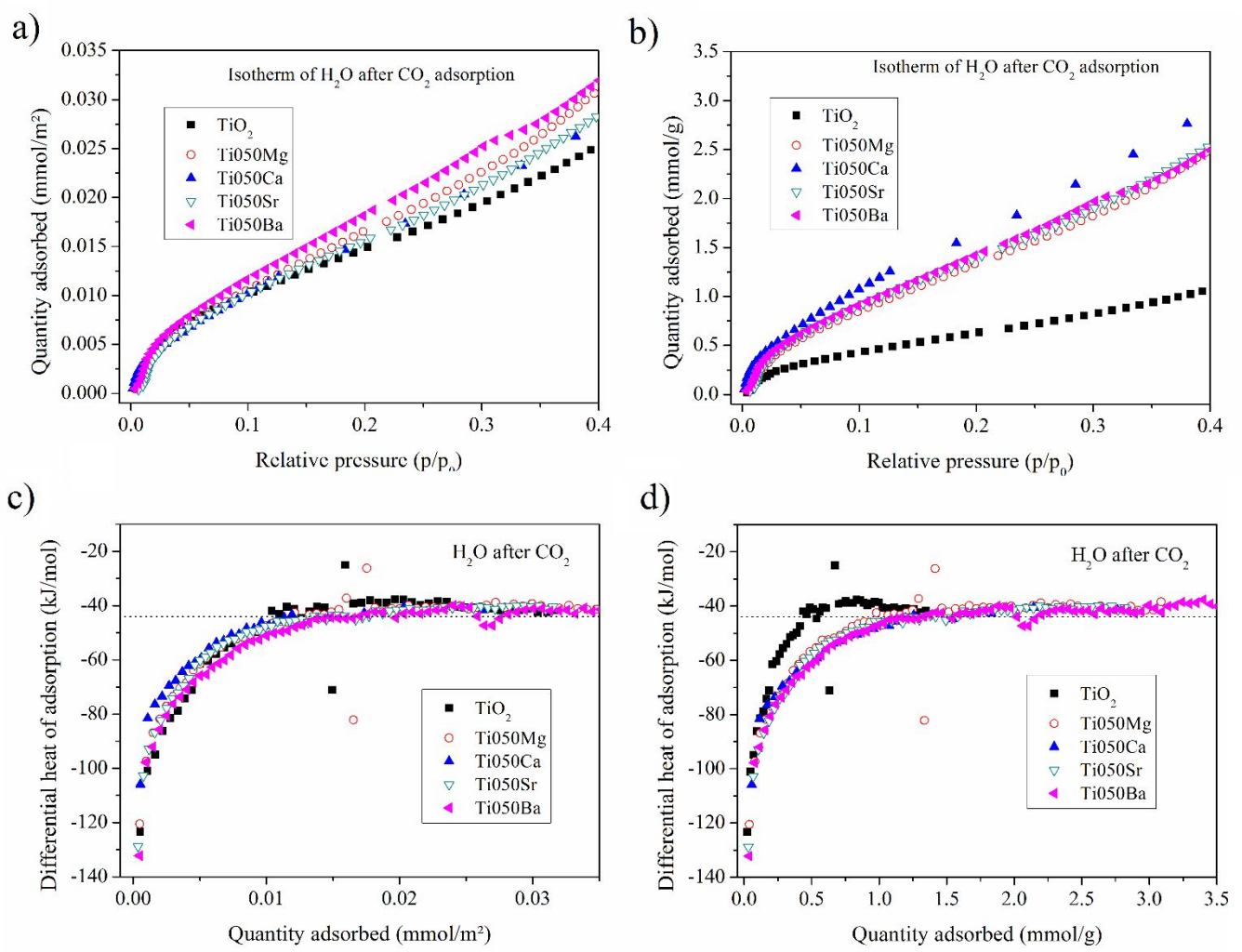

Fig. 4. Isotherm of H_2O adsorption normalized by surface area (a) and by weight (b). Differential heat of adsorption normalized by surface area (c) and by weight (d) for undoped TiO_2 and doped with 5 mol% MgO, CaO, SrO, and BaO.

CO_2 adsorption on TiO_2 is dependent on the surface defects and the crystal planes. It has been reported that defect-rich TiO_2 has superior adsorption than defect-free TiO_2. For instance, oxygen vacancy (V_o), which is influenced by the exposed crystal plane, can facilitate CO_2 adsorption and activation.[3] Thus, the differences observed from the data presented in this study and the one shown by Wu, et al.[30] could be related to process parameters of the TiO_2 nanopowders, including the type of synthesis, temperature and atmosphere during calcination, and precursors used. On the other hand, the increased adsorption shown by CaO-doped TiO_2 samples could be associated with the increase in the basicity of the surface due to CaO surface segregation. Basic surfaces, as the plane (001), adsorbs more CO_2 compared to

the (101) surface.[8] This is a result of the presence of more two-coordinated surface oxygen species (O_{2C}).

The H_2O adsorption isotherms and the differential heat of adsorption are shown in Fig. 4. The experiment was performed after the CO_2 adsorption. The chamber was evacuated for 6 h at room temperature before the H_2O adsorption. The objective was to evaluate the competition between the CO_2 and H_2O adsorption on doped and undoped TiO_2. Chemical identification of the post CO_2-adsorption surface was not performed because of how the equipment is setup, i.e. it was not possible to study the powder post CO_2 without exposing it to atmospheric air. However, we ensured the CO_2 adsorption based on previous literature that used mass spectroscopy.[32]

Table 3. Differential enthalpy for the first dose, integral enthalpy, amount of CO_2 adsorbed, surface coverage, and integral enthalpy for CO_2 and H_2O adsorption.

	CO_2 adsorption					H_2O adsorption				
Sample	Differential enthalpy for first dose (kJ/mol)	Integral enthalpy (kJ/mol CO_2)	Amount of CO_2 adsorbed (mmol/g)	Surface coverage (CO_2/nm²)	Integral enthalpy (J/m²)	Differential enthalpy for first dose (kJ/mol)	Integral enthalpy (kJ/mol H_2O)	Amount of H_2O adsorbed (mmol/g)	Surface coverage (H_2O/nm²)	Integral enthalpy (J/m²)
TiO_2	-50.4±0.3	-36.4±0.2	0.129±0.001	1.833±0.009	-0.111±0.001	-123.3±0.6	-68.2±0.3	0.440±0.002	6.259±0.031	-0.708±0.004
Ti050Mg	-51.3±0.3	-35.5±0.2	0.147±0.001	1.097±0.005	-0.065±0.001	-120.5±0.6	-62.6±0.3	0.979±0.005	7.303±0.037	-0.759±0.004
Ti050Ca	-62.6±0.3	-41.3±0.2	0.213±0.001	1.217±0.006	-0.083±0.001	-105.8±0.5	-59.9±0.3	1.195±0.006	6.827±0.034	-0.679±0.003
Ti050Sr	-50.3±0.3	-35.4±0.2	0.170±0.001	1.143±0.006	-0.067±0.001	-128.8±0.6	-61.0±0.3	1.215±0.006	8.183±0.041	-0.829±0.004
Ti050Ba	-49.9±0.3	-34.7±0.2	0.181±0.001	1.396±0.007	-0.080±0.001	-132.2±0.7	-60.5±0.3	1.330±0.007	10.250±0.051	-1.030±0.005

Two stages are observed in the H_2O adsorption isotherm curves. At very low relative pressures (<0.02), a swift increase in coverage as a function of pressure is seen. The differential enthalpies at this stage are very negative, which means a strongly exothermic reaction. Comparing these curves with previous studies, one sees a small difference in the curve shape at this first stage.[14,18,31] The slope of the curves is lower. In our previous study,[14] we have shown that this behavior is attributed to the type of pre-treatment the samples received before the H_2O adsorption, where O_2 in the pre-treatment decreases the surface defects resulting in a less reactive surface. Besides the slope of the curves, a small inflection is seen that was not observed in any of the previous studies with TiO_2. Gouvêa et al.,[32] have shown similar behavior with H_2O adsorption after CO_2 adsorption on ZnO nanoparticles. In their experiments, they connected a mass spectrometer to the manifold of the Micromeritics ASAP 2020. They found that this inflection was due to the release of CO_2 during the H_2O adsorption. Smith et al.[33] have also shown by TPD with sequential dosing of H_2O and CO_2 on TiO_2 that, independent of the dose order, H_2O molecules will displace CO_2 to occupy the highest energy binding sites available. In the same way, CO_2 adsorption on TiO_2 is greatly affected by introducing a water environment. In aqueous solution, CO_2 preferentially adsorbs at the bridging oxygen atom O_b, while Ti_{5C} sites are saturated by H_2O molecules that are difficult to displace.[34]

In the second stage, which is up to relative pressure of about 0.4, the behavior is similar to those presented in previous literature.[18,14,30] The slope of the isotherm curve is smaller, which indicates the formation of multiple water non dissociated layers.

From Fig. 4a,b, it is seen that the H_2O adsorption divided by surface area shows a small increase for doped samples comparing to undoped TiO_2, while H_2O adsorption normalized by weight increases the quantity adsorbed on doped powders by ~2-3 times per gram of material. This increase is associated with the increment in the SSA of the doped samples.

Differential enthalpies of water adsorption are more negative than those for CO_2 at all samples. This indicates a stronger interaction between H_2O and TiO_2, which confirms the preference of H_2O adsorption over CO_2. The differential enthalpy at the first dose for undoped TiO_2 was -123.3 kJ/mol, which is in agreement with previous studies.[14] No specific trend was observed in the differential enthalpy at the first dose for doped samples. The values varied from -105.8 kJ/mol to -132.2 kJ/mol. For the integral enthalpy of chemisorbed water on pristine TiO_2, our measurements gave -68.2 kJ/mol for a coverage of 6.26 H_2O/nm². For doped samples, the integral enthalpies were lower, being -62.6, -59.9, -61, and -60.5 kJ/mol for MgO, CaO, SrO, and BaO-doped TiO_2, respectively. However, the H_2O surface coverage for the same samples was higher than that for pristine TiO_2 (Table 3).

Conclusions

This journal is © The Royal Society of Chemistry 20xx

Please do not adjust margins

Energetics studies of CO_2 and H_2O adsorption on the surface chemistry modified TiO_2 with alkaline earth metals were performed. Significant amount of rigorous thermodynamic data on adsorption performance has been provided, offering opportunity for theoretical works with proper benchmark. The lixiviation process followed by thermal treatment under the oxygen atmosphere ensured the absence of organic and inorganic contaminants, assuring pristine clean samples proper for accurate and reliable experimental thermodynamic studies. The integral enthalpies of H_2O adsorption were more energetic than CO_2 adsorption in all compositions. The value for pure TiO_2 was -68.16 kJ/mol for a coverage of 6.25 H_2O/nm, while for doped samples were -62.6, -59.9, -61, and -60.5 kJ/mol for MgO, CaO, SrO, and BaO-doped TiO_2, respectively. The integral enthalpies of CO_2 adsorption were -36.4, -35.5, -41.3, -35.4, and -34.7 kJ/mol for pure TiO_2, MgO, CaO, SrO, and BaO-doped TiO_2, respectively. DRIFT measurements at 350 °C and 700 °C revealed higher amounts of CO_2 molecules adsorbed on modified TiO_2 nanoparticles. CO_2 adsorption associated with carbonates was removed from TiO_2 at temperatures ~500 °C to 600 °C, while linear CO_2 adsorption, vibration ~2330 cm^{-1}, remained on doped samples even at 700 °C.

In summary, TiO_2 modified with alkaline earth metals adsorbs more CO_2 than pristine TiO_2 mainly due to the increase in SSA. The enthalpy of CO_2 adsorption between undoped and doped TiO_2 has not changed significantly. However, the enthalpy of H_2O adsorption after CO_2 adsorption for alkaline earth doped TiO_2 was lower overall. This could benefit the CO_2 and H_2O co-adsorption, which could be an advantage in the AP process that needs both molecules to react to be converted to useful products, such as CH_4, CO, H_2, and CH_3OH. The increased CO_2 and H_2O adsorption and increased SSA benefit the catalytically assisted AP. However, further investigation should be performed on light absorption, charge separation, and selectivity to properly design the photocatalyst.

Conflicts of interest

There are no conflicts to declare.

Acknowledgements

D.G. would like to thank the financial support from FAPESP (proc. 2013/23209-2 and 2015/50443-1), the CNPq (proc. 4393352/2016-9) and LCT (Technologic characterization laboratory, USP, Poli, PMI). A.L.D acknowledges the CNPq and SHELL-RCGI (proj. 314131). RC thanks DMR Ceramics 1609781. A.N. acknowledges the U.S. Department of Energy Office of Basic Energy Sciences, grant DE-FG02-03ER46053, for support of the Peter A. Rock Thermochemistry Laboratory at UC Davis where the calorimetric experiments were performed.

Notes and references

1 D. C. Sorescu, S. Civiš and K. D. Jordan, *J. Phys. Chem. C,* 2014, **118** (3), 1628–1639.
2 P. Usubharatana, D. McMartin, A. Veawab and P. Tontiwachwuthikul, In *Industrial and Engineering Chemistry Research*, 2006, **45**, 2558–2568.
3 H. Zhao, F. Pan and Y. Li, *J. Mater.* 2017, **3** (1), 17–32.
4 H.-J. Freund and M. W. Roberts, *Surf. Sci. Rep.* 1996, **25** (8), 225–273.
5 T. Tachikawa, M. Fujitsuka and T. Majima, *J. Phys. Chem. C* 2007, **111** (14), 5259–5275.
6 A. L. da Silva, D. N. F. Muche, S. Dey, D. Hotza and R. H. R. Castro, *Ceram. Int.* 2016, **42** (4), 5113–5122.
7 X. Yang, C. Salzmann, H. Shi, H. Wang, M. L. H. Green and T. Xiao, *J. Phys. Chem. A* 2008, **112** (43), 10784–10789.
8 U. Tumuluri, J. D. Howe, W. P. Mounfield, M. Li, M. Chi, Z. D. Hood, K. S. Walton, D. S. Sholl, S. Dai and Z. Wu, *ACS Sustain. Chem. Eng.* 2017, **5** (10), 9295–9306.
9 A. Parameswari, Y. Soujanya and G. N. Sastry, *J. Phys. Chem. C* 2019, **123** (110), 3491–3504.
10 A. Markovits, A. Fahmi and C. Minot, *J. Mol. Struct. THEOCHEM* 1996, **371**, 219–235.
11 L. Liu and Y. Li, *Aerosol Air Qual. Res.* 2014, **14** (2), 453–469.
12 L. Liu, C. Zhao, D. Pitts, H. Zhao and Y. Li, *Catal. Sci. Technol.* 2014, **4** (6), 1539–1546.
13 F. Wang, Y. Zhou, P. Li, L. Kuai and Z. Zou, *Chinese J. Catal.* 2016, **37** (6), 863–868.
14 A. L. da Silva, D. N. F. Muche, L. B. Caliman, J. Bettini, R. H. R. Castro, A. Navrotsky and D. Gouvêa, *J. Phys. Chem. C* 2019, **123** (8), 4949–4960.
15 R. A. M. P. de Oliveira, A. L. da Silva, L. B. Caliman and D. Gouvêa, *Ceram. Int.* 2020, **46**, 10555–10560.
16 A. A. Bernardes, L. B. Caliman, A. L. da Silva, J. Bettini, K. L. Guimarães and D. Gouvea, *J. Am. Ceram. Soc.* 2020, **103**, 2835–2844.
17 R. H. R. Castro and D. V. Quach, *J. Phys. Chem. C* 2012, **116** (46), 24726–24733.
18 A. L. da Silva, D. Hotza and R. H. R. Castro, *Appl. Surf. Sci.* 2017, **393**, 103–109.
19 L. Wu, S. Dey, M. Gong, F. Liu and R. H. R. Castro, *J. Phys. Chem. C* 2014, **118** (51), 30187–30196.
20 R. H. R. Castro, Overview of Conventional Sintering. In: R. H. R. Castro and K. van Benthem (eds), Sintering. Engineering Materials, Springer, Berlin, Heidelberg, 2012, **35**, 1–16.
21 H. Gandelman, A. L. da Silva, L. B. Caliman and D. Gouvêa, *Ceram. Int.* 2018, **44** (10), 11390–11396.
22 H. Zhang and J. F. Banfield, *Chem. Rev.* 2014, **114** (19), 9613–9644.
23 B. Bokhimi, A. Morales, O. Novaro, T. López, E. Sánchez and R. Gómez, *J. Mater. Res.* 1995, **10** (11), 2788–2796.
24 H. Zhang, B. Chen and J. F. Banfield, *Phys. Chem. Chem. Phys.* 2009, **11** (14), 2553–2558.
25 G. Li, L. Li, J. Boerio-Goates and B. F. Woodfield, *J. Am. Chem. Soc.* 2005, **127** (24), 8659–8666.
26 V. Swamy, D. Menzies, B. C. Muddle, A. Kuznetsov, L. S. Dubrovinsky, Q. Dai and V. Dmitriev, *Appl. Phys. Lett.* 2006, **88** (24), 243103.
27 J. L. Mi, C. Clausen, M. Bremholm, N. Lock, K. M. A. Jensen, M. Christensen and B. B. Iversen, *Cryst. Growth Des.* 2012, **12** (12), 6092–6097.
28 J. R. Eltzholtz, C. Tyrsted, K. M. Ø. Jensen, M. Bremholm, M. Christensen, J. Becker-Christensen and B. B. Iversen, *Nanoscale* 2013, **5** (6), 2372–2378.
29 Z. Matěj, L. Matějová and R. Kužel, XRD Analysis of Nanocrystalline Anatase Powders Prepared by Various Chemical Routes: Correlations between Micro-Structure and Crystal Structure Parameters. In *Powder Diffraction*; Cambridge University Press, 2013, **28**, S161–S183.
30 L. Wu, X. Guo and A. Navrotsky, *Am. Mineral.* 2019, **104** (5), 686–693.

31 J. Miagava,; A. L. da Silva, A. Navrotsky, R. H. R. Castro and D. Gouvêa, *Journal of the American Ceramic Society*. 2016, **99**, 638–644.
32 D. Gouvêa, S. V. Ushakov and A. Navrotsky, *Langmuir* 2014, **30** (30), 9091–9097.
33 R. S. Smith, Z. Li, L. Chen, Z. Dohnálek and B. D. Kay, *J. Phys. Chem. B* 2014, **118** (28), 8054–8061.
34 K. Klyukin and V. Alexandrov, *J. Phys. Chem. C* 2017, **121** (19), 10476–10483.

This journal is © The Royal Society of Chemistry 20xx

Please do not adjust margins

Table of content

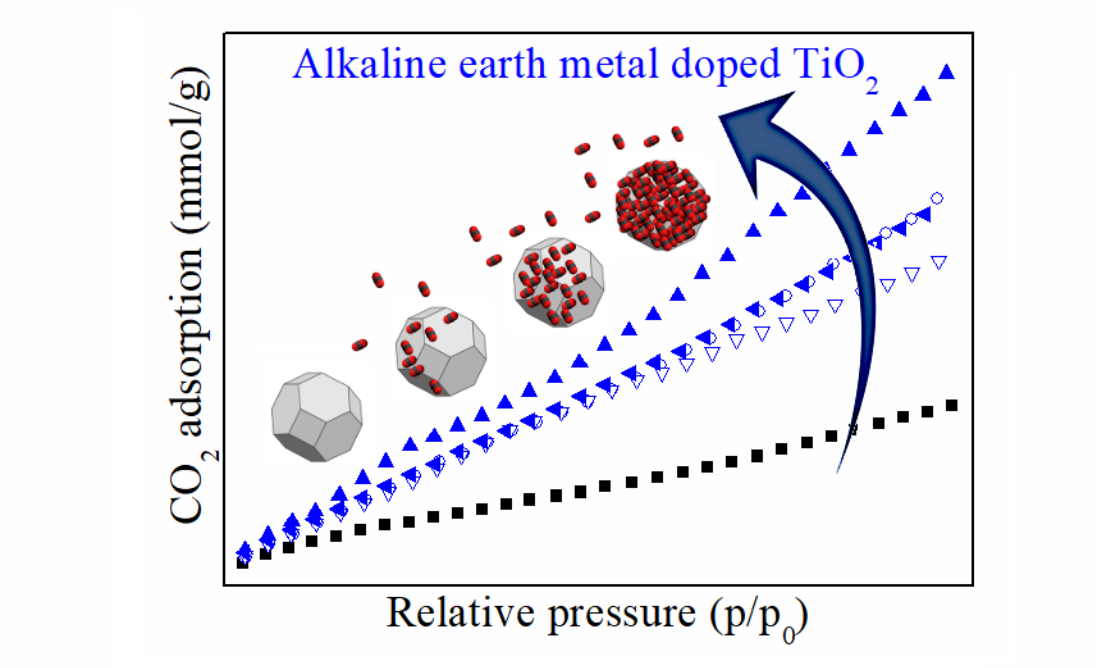

Highlight of the novelty of the work:

CO_2 and H_2O adsorption on TiO_2 nanocatalyst has improved due to the surface segregation of alkaline earth metals.